Resistivity profiles in multicrystalline silicon ingots featuring gallium co-doping

Rune Søndenå, Halvard Haug, Adolphus Song, Chen-Chih Hsueh, and Jan Ove Odden

Citation: AIP Conference Proceedings **1999**, 130016 (2018); doi: 10.1063/1.5049335
View online: https://doi.org/10.1063/1.5049335
View Table of Contents: http://aip.scitation.org/toc/apc/1999/1
Published by the American Institute of Physics

Articles you may be interested in

Impact of thermal history on defects formation in the last solid fraction of Cz silicon ingots
AIP Conference Proceedings **1999**, 130012 (2018); 10.1063/1.5049331

Elimination of BO-LID in mass production using illuminated annealing in a coupled firing and regeneration tool
AIP Conference Proceedings **1999**, 130002 (2018); 10.1063/1.5049321

Temperature coefficients in compensated silicon solar cells investigated by temperature dependent lifetime measurements and numerical device simulation
AIP Conference Proceedings **1999**, 020010 (2018); 10.1063/1.5049249

Understanding the optics of industrial black silicon
AIP Conference Proceedings **1999**, 050007 (2018); 10.1063/1.5049297

Opto-electrical simulation of III-V nanowire based tandem solar cells on Si
AIP Conference Proceedings **1999**, 120001 (2018); 10.1063/1.5049318

Thermal stability analysis of WO_x and MoO_x as hole-selective contacts for Si solar cells using in situ XPS
AIP Conference Proceedings **1999**, 040027 (2018); 10.1063/1.5049290

AIP | Conference Proceedings
Get 30% off all print proceedings!
Enter Promotion Code PDF30 at checkout

Resistivity Profiles in Multicrystalline Silicon Ingots Featuring Gallium Co-doping

Rune Søndenå[1, a)], Halvard Haug[1], Adolphus Song[2], Chen-Chih Hsueh[2], and Jan Ove Odden[3]

[1]*Institute for Energy Technology, Instituttveien 18, 2007 Kjeller, Norway*
[2]*REC Solar, 20 Tuas South Ave 14, Singapore*
[3]*REC Solar Norway, Fiskaaveien 100, 4621 Kristiansand S, Norway*

[a)]Corresponding author: rune.sondena@ife.no

Abstract. Three ingots with different doping concentrations have been produced using Elkem Solar Silicon feedstock. Gallium dopants are added to the compensated Elkem Solar Silicon ingots in order to obtain a more uniform resistivity profile throughout the heights, and to avoid a change from p-type to n-type silicon towards the top of the ingots. In addition a reference ingot based on non-compensated silicon has been cast. The resistivity profiles along the height of these ingots are determined using Eddy current measurements on the sides of center blocks. Corresponding resistivity profiles are then estimated using the concentration of dopants in the melt, the Scheil equation, and the numerical device simulation software PC1Dmod6.2. The implementation of advanced c-Si models accounting for changes in the carrier mobility and incomplete ionization of dopants due to the compensation doping were found to be necessary to correctly explain the observations. Using this approach, it was possible to reproduce the experimentally obtained resistivity profiles using slightly modified values for the segregation coefficients. New effective segregation coefficients for B and Ga are proposed.

INTRODUCTION

The Elkem Solar process route for solar grade silicon feedstock production is based on the chemical route, including purification steps such as slag treatment and leaching. As the chemical purification route does not include silicon in a gaseous phase less energy is used in this purification process than through the conventional Siemens process.[1–3] The main difference between conventional feedstock and Elkem Solar Silicon (ESS™) is the presence of phosphorus in addition to the boron in the latter. These extra phosphorus dopants are compensated for by the elevated boron levels, hence the term compensated silicon. 100% ESS™ typically contains 0.6 ppmw phosphorus.[4] The addition of a third dopant in the melt, the acceptor gallium, results in less variation in the net doping after solidification and therefore also less variation in the resistivity over the ingot height. In addition the transition from p-type material to n-type material often observed towards the top of ingots containing boron and phosphorus can be avoided.[5] Thus, compensation engineering using gallium co-doping, also called tri-doping, both minimizes the resistivity range throughout the ingot and increases the yield considerably when casting ingots based on compensated silicon feedstock.

Dopant and impurity concentrations are known to vary over the ingot height due to segregation. Boron, phosphorus and gallium concentrations will all increase with increasing height in the ingot, while the oxygen content tend to decrease.[6] This segregation of species between the liquid and the solid phases of silicon is controlled by the segregation coefficient. The concentration of each dopant or impurity element throughout the height of a crystal is described by the Scheil equation:

$$C_S(x) = k_{eff.}C_0(1-x)^{(k_{eff.}-1)} \tag{1}$$

SiliconPV 2018, The 8th International Conference on Crystalline Silicon Photovoltaics
AIP Conf. Proc. 1999, 130016-1–130016-6; https://doi.org/10.1063/1.5049335
Published by AIP Publishing. 978-0-7354-1715-1/$30.00

where $C_s(x)$ is the impurity concentration in the solid at a relative height x, C_0 is the initial impurity concentration in the melt and $k_{eff.}$ is the effective segregation coefficient. The thermal gradient, shape and thickness of the solid liquid interface as well as the convection in the melt may affect the effective segregation coefficient. In Czochralski silicon (Cz-Si) the rotation of the crucible and crystal may also have an impact. It has also been shown that the effective segregation coefficients for boron and gallium is affected by the total acceptor concentration when they occur together in silicon, but mainly for total acceptor concentrations over 10^{17} cm^{-3}.[7] The efficient segregation coefficient is typically a bit smaller that k_0 and depends on the growth rate, v, the boundary layer thickness, d, and the diffusivity of impurity species in the molten phase, D.[8,9]

$$k_{eff.} = \frac{k_0}{k_0 + (1 - k_0)e^{\left(\frac{-v \cdot \delta}{D}\right)}} \tag{2}$$

Experimental and theoretical segregation coefficients for the three dopant elements are shown in Table 1.

TABLE 1. Experimental and theoretical segregation coefficients for B, P and Ga. Values for k_0 and $k_{eff.}$ for multicrystalline silicon as well as for Czhochralski silicon are included.

Element	k_0 or $k_{eff.}$	Comment
B	0.8	k_0 [10]
	0.751	$k_{eff.}$ Cz-Si, rotation dependence[11]
	0.716	k_0 Cz-Si[11]
	0.757	$k_{eff.}$ [12]
	0.72	$k_{eff.}$ Cz-Si, doping dependent[7]
	0.75	$k_{eff.}$ Cz-Si[13]
	0.65	$k_{eff.}$ multicrystalline silicon[8]
	0.75 - 0.77	$k_{eff.}$ present work
P	0.35	k_0 [10]
	0.25	k_0 Cz-Si, rotation dependent[9]
	0.32-0.36	$k_{eff.}$[9]
	0.41	$k_{eff.}$ Cz-Si[13]
	0.31	$k_{eff.}$ present work
Ga	0.008	k_0[10]
	0.008	k_0 Cz-Si, doping dependent[7,14]
	0.0086	$k_{eff.}$ multicrystalline silicon[15]
	0.0070 - 0.0078	$k_{eff.}$ present work

PC1D is an efficient one-dimensional semiconductor device simulator which is widely used in the solar cell research community.[16,17] However, models for various physical properties of crystalline silicon have been refined and improved since the latest official release of PC1D in 1997. In addition the computational power of an average computer has increased allowing for heavier calculations. The physics engine of PC1D has therefore been updated the last few years in order to implement updated models; Fermi-Dirac statistics and corresponding models for band-gap-narrowing, models for carrier mobility, carrier recombination models, and incomplete ionization of dopants.[18–21] The compensation level and the increased total number of dopants in compensated silicon will affect several physical properties. Among the more important effects are the slightly reduced carrier mobility and the incomplete ionization of the dopants. These two effects are accounted for in the most recent version, namely PC1Dmod6.2,[21] by the inclusion of Schindler's unified model for mobility in compensated silicon[22] and Altermatt's models for incomplete ionization.[23,24]

In the present work PC1Dmod6.2 has been used to simulate the resistivity profiles throughout the full height of four different silicon ingots. The simulated resistivity curves are compared to measured values and effective segregation coefficients are proposed.

EXPERIMENTAL DETAILS

Four different high performance multicrystalline (HPMC) silicon ingots were investigated in this work. Ingots with target resistivities of 0.5, 0.9 and 1.3 Ω-cm were produced using gallium co-doped ESS™, using a blend of 70%

Elkem Solar Silicon and 30% polysilicon. Using tri-doping, i.e. adding boron and gallium in addition to dopants already present in the compensated silicon feedstock, each dopant profile has been engineered to be as flat as possible. In addition a non-compensated ingot with a target resistivity of 1.3 Ω-cm, made with a blend of polysilicon and fluidized bed reactor (FBR) silicon feedstock, was cast as a reference. The resistivity profile was determined by performing Eddy current measurements along the height of one block prior to wafering.

Doping profiles are estimated using the Scheil equation (Eq. 1) together with the dopant concentrations in the charge. The phosphorus and the gallium concentrations are considered fixed and identical for the three ingots based on the expected purity level of ESS™ feedstock and the amount of gallium added to the charge, while the boron content is adjusted to obtain the different target resistivity values. Using a slightly altered version of the device simulation tool PC1Dmod6.2, allowing for the calculation of dopant ionization in tri-doped silicon, resistivity profiles for all four ingots was calculated based on the doping profiles from Eq. 1.[25] The optimal boron concentration for each ingot is found by least square fitting towards the measured resistivity profiles. Least square fitting is also performed in order to find a set of effective segregation coefficients best suited to describe the resistivity profiles in our ingots.

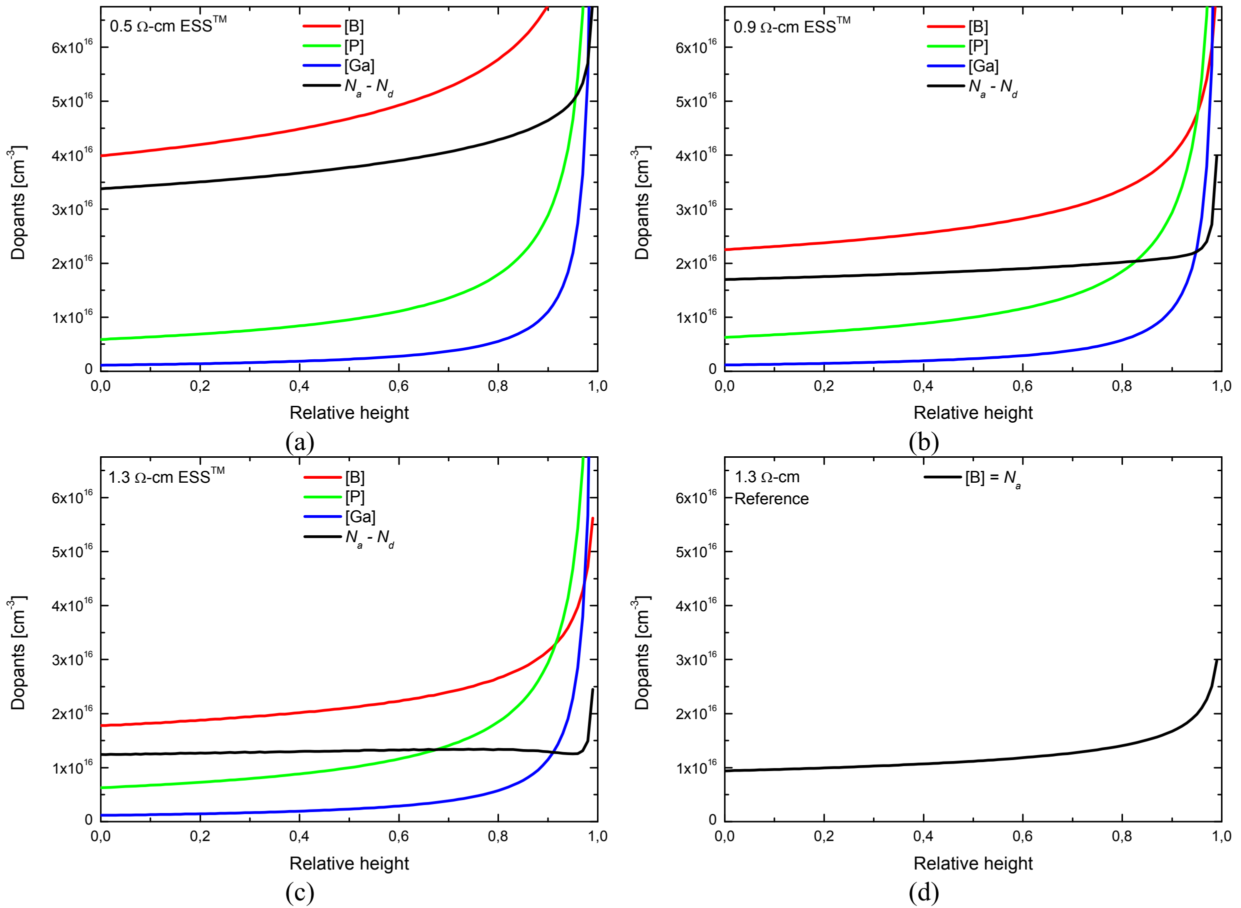

FIGURE 1. Dopant profiles for B, P and Ga throughout the height in Ga co-doped HPMC silicon ingots based on the initial concentrations of dopants added to the melt and the Scheil equation. Effective segregation coefficients proposed in this paper are used.

TABLE 2. Initial impurity concentrations in the melt, C_0, based on expected levels in the feedstock material, and least square fitting towards measured resistivity data. Effective segregation coefficients have been used in fitting procedure.

Ingot	P [cm^{-3}]	B [cm^{-3}]	Ga [cm^{-3}]
0.5 Ω-cm ESS™	1.9e16	5.2e16	1.6e17
0.9 Ω-cm ESS™	1.9e16	3.0e16	1.6e17
1.3 Ω-cm ESS™	1.9e16	2.4e16	1.6e17
1.3 Ω-cm poly/FBR Reference	-	1.3e16	-

RESULTS AND DISCUSSION

The dopant profiles and the net doping N_a-N_d, according to the Scheil equation and effective segregation coefficients, are shown in Fig. 1. Effective segregation coefficients and the dopant concentrations used in the optimization are shown in Table 1 and 2, respectively. The net doping of the 0.9 and 1.3 Ω-cm tri-doped ingots both show less variation of the resistivity over the height than the non-compensated reference. The exception is in the top 2-3 % of these two ingots where there is a very sharp increase in N_a-N_d. Hence by using gallium co-doped ESS^{TM} for the 0.9 and the 1.3 Ω-cm ingots the resistivity range of the resulting wafers is narrower than for a non-compensated reference ingot with comparable resistivity. The 0.5 Ω-cm ingot on the other hand show a larger span in the net doping than the reference ingot. The dopant profiles for all three compensated ingots also show that the phosphorus concentration exceeds the boron concentration at about 90 to 95% of the ingot height. In conventional compensated silicon, i.e. without gallium co-doping, this would lead to a change from p-type to n-type silicon. However, with compensation engineering this transition is completely avoided, increasing the yield considerably.

Figure 2 shows the estimated incomplete ionization of dopants for all the ingots. In the highly doped ingot with a resistivity of 0.5 Ω-cm, about 4% of the dopants are non-ionized at the bottom of the ingot. About 2% of the dopants are not ionized in the bottom of the other three ingots. With increasing total amounts of dopants present towards the top of the ingots the fraction of incomplete ionization among the dopant species increases as well. The increase of total dopants towards the top of the compensated ingots is much larger than the corresponding increase in the reference, and this is reflected in a much larger fraction of non-ionized dopants towards the top of the ESS^{TM}-ingots.

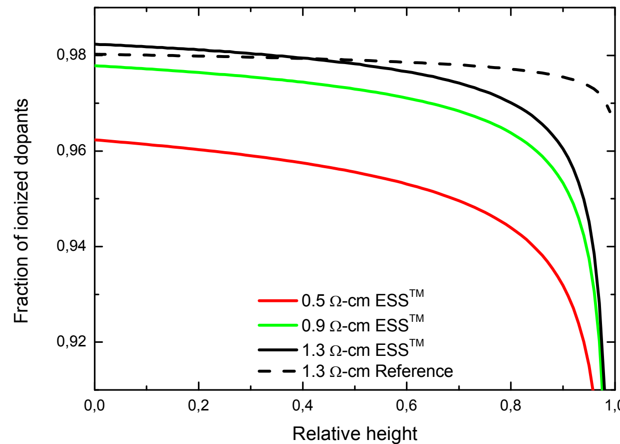

FIGURE 2. Incomplete ionizations of the dopant atoms according to the model of Altermatt et al. implemented in PC1Dmod6.2.

Modelled and measured resistivity profiles as a function of ingot height are shown in Fig. 3. A general decrease in the resistivity with increasing height is observed in the 0.5 Ω-cm ingot. Towards the top of the ingot, at about 95-97% of the height, a small peak with increased resistivity is observed in the measured data. Interestingly this feature can also be reproduced in the simulated curve. Both the 0.9 and the 1.3 Ω-cm ingots show a decrease of the resistivity in the bottom half of the ingot and a sharper increase toward the very top. It is impossible to make perfect fits to measured profiles using the generally accepted segregation coefficients (i.e. values from Trumbore). This is especially visible in the 0.9 Ω-cm ingot shown in Fig. 3b. However, it was found that minor changes to the effective segregation coefficients greatly improve the fit between simulated and measured resistivity profiles. New segregation coefficients for compensated Si are therefore proposed here, given in Table 1. Using these values, the measured resistivity profiles can be reproduced almost perfectly, as shown in Fig. 3. It is to a certain degree possible to obtain a good fit to the measured resistivity data assuming 100% ionization of dopants and Klaassens resistivity model simply by adjusting the $k_{eff.}$-values. However, with the implementation of state-of-the-art physical models implemented in PC1Dmod6.2, effective segregation coefficients closer to Trumbores k_0-values can be used. The non-compensated reference ingot is equally well described with the commonly used values for $k_{0,B}$ and our proposed value for $k_{B,eff.}$ of 0.75.

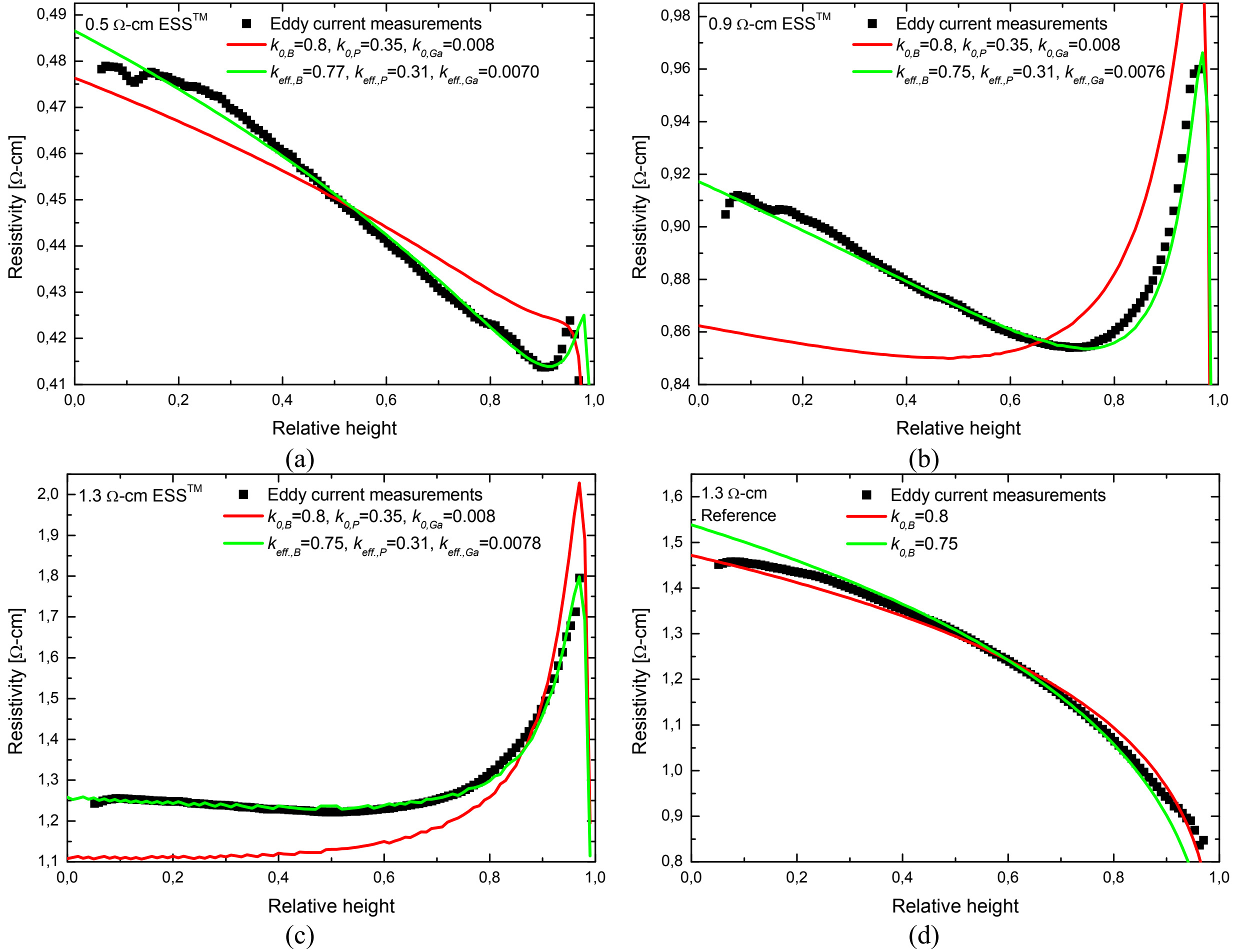

FIGURE 3. Measured and modelled resistivity curves as a throughout the height in ingots with target resistivity of 0.5, 0.9, and 1.3 Ω-cm are shown in a, b, and c, respectively. The non-compensated reference is shown in d. Resistivity curves based on conventional and proposed segregation coefficient are shown in red and green, respectively, while measured date are shown with black symbols.

SUMMARY

Doping profiles throughout the height of HPMC silicon ingots containing boron, phosphorus and gallium have been estimated sung the Scheil equation. The initial concentrations of dopants are based on the expected levels in the feedstock as well as least square fitting against measured resistivity curves. Effects of incomplete ionization for high concentrations of dopants as well as the effect of compensation on the charge carrier mobility are accounted for in the numerical simulation tool PC1Dmod6.2.

The conventional k_0-values from Trumbore fail to accurately describe different features of the measured resistivity curves for the compensated ingots with different doping levels, but fits reasonably well for the non-compensated ingot. However, by introducing effective segregation coefficients the agreement between measured and simulated resistivity curves can be increased considerably. Effective segregation coefficients for our ingots based on ESS™ feedstock are therefore proposed.

ACKNOWLEDGMENTS

Funding for this work was provided through the EnergiX programme of the Norwegian Research Council, project number 256271 - Performance and Reliability IN Compensated Elkem Solar Silicon.

REFERENCES

1. R. Glöckner, J.O. Odden, G. Halvorsen, R. Tronstad, and M.J. de Wild-Scholten, "Environmental life cycle assessment of the Elkem Solar metallurgical process route to solar grade silicon with focus on energy consumption and greenhouse gas emissions", in *Silicon Chem. Sol. Ind. IX* (Oslo, Norway, 2008).
2. M.J. de Wild-Scholten and R. Gløckner, "Environmental footprint of Elkem Solar Silicon®", in *Silicon Chem. Sol. Ind. XI* (Bergen-Ulvik, Norway, 2012).
3. A.-K. Søiland, J.O. Odden, B. Sandberg, K. Friestad, J. Håkedal, E. Enebakk, and S. Braathen, "Solar silicon from a metallurgical route by Elkem Solar - A viable alternative to virgin polysilicon", in *CSSC-6* (Aix-Les-Bains, France, 2012).
4. J.O. Odden, T.C. Lommasson, M. Tayyib, J. Vedde, T. Buseth, K. Friestad, H. Date, and R. Tronstad, Sol. Energy Mater. Sol. Cells **130**, 673-678 (2014).
5. A. Cuevas, M. Forster, F. Rougieux, and D. Macdonald, Energy Procedia **15**, 67-77 (2012).
6. K. Tang, M. Syvertsen, R. Fagerberg, C. Modanese, and M. Di Sabatino, "Oxygen distribution in directionally solidified multicrystalline silicon", in *CSSC-6* (Aix-Les-Baines, France, 2012).
7. S. Uda, X. Huang, M. Arivanandhan, and R. Gotoh, "Enhancement of Ga doping in Czochralaki-grown Si crystal by B- codoping", in *5th Int. Symp. Adv. Sci. Technol. Silicon Mater.* (Kona, Hawaii, 2008).
8. D. Macdonald, A. Cuevas, A. Kinomura, Y. Nakano, and L.J. Geerligs, J. Appl. Phys. **97**, 33523 (2005).
9. K. Tang, E.J. Øvrelid, G. Tranell, and M. Tangstad, J. Miner. Met. Mater. Soc. **61**, 49-55 (2009).
10. F.A. Trumbore, Bell. Sys. Tech. J. **39**, 205-233 (1960).
11. B.-C. Sim, K.-H. Kim, and H.-W. Lee, J. Cryst. Growth **290**, 665-669 (2006).
12. K. Tang, E.J. Øvrelid, G. Tranell, and M. Tangstad, Mater. Trans. **50**, 1978-1984 (2009).
13. C. Sun, H.T. Nguyen, H.C. Sio, F.E. Rougieux, and D. Macdonald, IEEE J. Photovolt. **7**, 988-995 (2017).
14. X. Huang, M. Arivanandhan, R. Gotoh, T. Hoshikawa, and S. Uda, J. Cryst. Growth **310**, 3335-3341 (2008).
15. A.A. Betekbaev, B.N. Mukashev, L. Pelissier, P. Lay, G. Fortin, L. Bounaas, D.M. Skakov, and A.A. Pavlov, Mod. Electron. Mater. **2**, 61-65 (2016).
16. D.A. Clugston and P.A. Basore, "PC1D version 5: 32-bit solar cell modeling on personal computers", in *26th IEEE PVSC* (New York, New York, 1997), pp. 207–210.
17. P.A. Basore, IEEE Trans. Electron Devices **37**, 337 (1990).
18. H. Haug, B.R. Olaisen, Ø. Nordseth, and E.S. Marstein, Energy Procedia **38**, 72-79 (2013).
19. H. Haug, A. Kimmerle, J. Greulich, A. Wolf, E. Stensrud Marstein, and E.S. Marstein, Sol. Energy Mater. Sol. Cells **131**, 30-36 (2014).
20. H. Haug, J. Greulich, A. Kimmerle, and E.S. Marstein, Sol. Energy Mater. Sol. Cells **142**, 47-53 (2015).
21. H. Haug and J. Greulich, Energy Procedia **92**, 60-68 (2016).
22. F. Schindler, M. Forster, J. Broisch, J. Schön, J. Giesecke, S. Rein, W. Warta, and M.C. Schubert, Sol. Energy Mater. Sol. Cells **131**, 92-99 (2014).
23. P.P. Altermatt, A. Schenk, and G. Heiser, J. Appl. Phys. **100**, 113714 (2006).
24. P.P. Altermatt, A. Schenk, B. Schmithüsen, and G. Heiser, J. Appl. Phys. **100**, 113715 (2006).
25. M. Forster, A. Cuevas, E. Fourmond, F.E. Rougieux, and M. Lemiti, J. Appl. Phys. **111**, 43701 (2012).